INFLUENCE OF BASSET HISTORY FORCE ON PREFERENTIAL CONCENTRATION OF SMALL PARTICLES AND BUBBLES IN TURBULENCE

SATOSHI YOKOJIMA
Department of Mathematical and Systems Engineering, Shizuoka University, Hamamatsu, Japan, yokojima@shizuoka.ac.jp

YOSHIAKI SHIMADA
Department of Mathematical and Systems Engineering, Shizuoka University, Hamamatsu, Japan

KAZUKI MUKAIYAMA
Department of Mathematical and Systems Engineering, Shizuoka University, Hamamatsu, Japan

ABSTRACT

Computation of the Basset history force can be very expensive, and hence, in past studies, either the whole part or some fraction of the history has been neglected even in the cases where its contribution may be important. Here the effects of the Basset history force on preferential concentration of small particles in a homogeneous isotropic turbulence under a wide range of the particle-to-fluid mass density ratio (from 0 up to 10000) have been investigated by direct simulations of the Navier-Stokes equations. The Basset force is numerically approximated by the method of van Hinsberg et al. (J. Comput. Phys. 230 (2011) 1465). Compared with the traditional window method where the Basset integral is evaluated only over the latest period of size $t_{\rm win}$, the method of van Hinsberg that approximates the tail of the Basset force kernel by exponential functions is found to give a better result by using a much shorter (typically, two-order-of-magnitude smaller) $t_{\rm win}$. It is clearly revealed that the presence of the Basset force weakens the level of preferential concentration to some extent, especially under the conditions of the mass density ratio of around $1.5-10$ for heavy particles and smaller than 0.7 for light particles.

Keywords: Preferential concentration, Basset history force, light and heavy particles, homogeneous isotropic turbulence, direct numerical simulation

1. INTRODUCTION

The motion of a small isolated rigid spherical particle in a non-uniform velocity field is well described by the Maxey-Riley (MR) equation (Maxey and Riley, 1983):

$$\begin{aligned} m_{\rm p}\frac{d\mathbf{u}_{\rm p}}{dt} =& 6\pi a\mu(\mathbf{u}_{\rm f}-\mathbf{u}_{\rm p}) + m_{\rm f}\frac{D\mathbf{u}_{\rm f}}{Dt} - (m_{\rm p}-m_{\rm f})g\mathbf{e}_z + \frac{1}{2}m_{\rm f}\left(\frac{D\mathbf{u}_{\rm f}}{Dt}-\frac{d\mathbf{u}_{\rm p}}{dt}\right) \\ &+ 3\sqrt{3\mu a m_{\rm f}}\int_{\tau=-\infty}^{t}\frac{1}{\sqrt{t-\tau}}\left(\frac{d\mathbf{u}_{\rm f}}{d\tau}-\frac{d\mathbf{u}_{\rm p}}{d\tau}\right)\mathrm{d}\tau. \end{aligned} \tag{1}$$

Here a denotes the particle radius, $m_{\rm p}$ the particle mass, $\mathbf{u}_{\rm p}$ the particle velocity, $\mathbf{u}_{\rm f}(\mathbf{x},t)$ the fluid velocity, μ the dynamic fluid viscosity, $m_{\rm f}$ the mass of fluid element with a volume equal to that of the particle, g the gravitational acceleration, and $\mathbf{e}_z$ the unit vector in the opposite direction of the gravitational force. The last term on the RHS denotes the Basset history force, the most time- and memory-consuming part. Hence, in past studies, either the whole part or some fraction of the history has been neglected even in the cases where its contribution may be important.

By splitting the added mass term, the equation can be rewritten as (see van Hinsberg et al. (2017))

$$\frac{d\mathbf{u}_{\rm p}}{dt} = \frac{\mathbf{u}_{\rm f}-\mathbf{u}_{\rm p}}{\tau_{\rm p}^*} + \beta\frac{D\mathbf{u}_{\rm f}}{Dt} - (1-\beta)g\mathbf{e}_z + \sqrt{\frac{3\beta}{\pi\tau_{\rm p}^*}}\int_{\tau=-\infty}^{t}\frac{1}{\sqrt{t-\tau}}\left(\frac{d\mathbf{u}_{\rm f}}{d\tau}-\frac{d\mathbf{u}_{\rm p}}{d\tau}\right)\mathrm{d}\tau, \tag{2}$$

where $\beta\equiv 3/(2\gamma+1)$, $\gamma\equiv m_{\rm p}/m_{\rm f}$, $\tau_{\rm p}^*\equiv(3\tau_{\rm p}/(3-\beta))$, and $\tau_{\rm p}(\equiv m_{\rm p}/(6\pi a\mu))$ is the particle response time. It is noteworthy that the pressure-gradient force (the second term on the RHS of eq. (2)) $\mathbf{f}_{\rm P}$ and

Table 1. Relation among β, $\sqrt{\beta}$, and the particle-to-fluid mass density ratio γ.

γ	∞	1000	100	10	3	1	0.9	0.5	0.1	0.01	0
β	0	0.0015	0.0149	0.1429	0.4285	1	1.0714	1.5000	2.5000	2.9412	3
$\beta^{1/2}$	0	0.0387	0.1222	0.3780	0.6547	1	1.0351	1.2247	1.5811	1.7150	1.7321

the Basset force (the last term) $\mathbf{f}_{\mathrm{B}}$ are proportional to β and $\sqrt{\beta}$, respectively. Table 1 shows how β and $\sqrt{\beta}$ behave as a function of γ, the particle-to-fluid mass density ratio. When the particle is much heavier than the surrounding fluid (i.e., $\gamma \to \infty$), only the Stokes drag force $\mathbf{f}_{\mathrm{St}}$ and the gravity force $\mathbf{f}_{\mathrm{G}}$ remain on the RHS of eq. (2). With decrease in γ, $\mathbf{f}_{\mathrm{B}}$ first starts to compete with $\mathbf{f}_{\mathrm{St}}$ and $\mathbf{f}_{\mathrm{G}}$. When decreasing γ even further, $\mathbf{f}_{\mathrm{P}}$ also becomes important. In section 2.2, an example where this argument does hold is presented.

Here we examine the impact of the Basset history force on preferential concentration of small particle (i.e., the accumulation of particles within specific regions of instantaneous turbulence fields) in a homogeneous isotropic turbulence. The mass density ratio γ is changed systematically from 0 (ultimately light particle compared with the surrounding fluid) up to 10000 (significantly heavy particle). The Basset force is approximately computed by the method of van Hinsberg et al. (2011), whose essential characteristic is to approximate the tail of the Basset force kernel by exponential functions.

2. APPROXIMATION TO BASSET HISTORY FORCE AND ITS VALIDATION

2.1 Approximation to Basset history force

We employed the method proposed by van Hinsberg et al. (2011) to calculate the Basset history force. Here the method is described briefly. For further details, the reader is referred to the paper.

To simplify the mathematical expression, we introduce the following variables and functions: $\mathbf{f} \equiv \mathbf{u}_{\mathrm{f}} - \mathbf{u}_{\mathrm{p}}$, $\mathbf{g} \equiv \mathrm{d}\mathbf{f}(\tau)/\mathrm{d}\tau$, $K_{\mathrm{B}}(t) \equiv 1/\sqrt{t}$, and $c'_{\mathrm{B}} \equiv \sqrt{(3\beta)/(\pi\tau^*_{\mathrm{p}})}$. Then the Basset history force appearing in eq. (2) can be rewritten as

$$\mathbf{f}_{\mathrm{B}}(t) = c'_{\mathrm{B}} \int_{\tau=-\infty}^{t} K_{\mathrm{B}}(t-\tau)\mathbf{g}(\tau)\mathrm{d}\tau. \tag{3}$$

The main difficulty in computing the Basset force can be attributed to the fact that the values of $\mathbf{g}(\tau)$ of all the particles need to be hold over $\tau \in [-\infty, t]$ and that the integral appearing in eq. (3) needs to be calculated at every time step. Therefore, in most of the past studies that took the Basset force into account, the integral was evaluated only over the latest period of size t_{win} (e.g., Sugiyama et al., 2004; Bombardelli et al., 2008):

$$\mathbf{f}_{\mathrm{B}}(t) \approx \mathbf{f}_{\mathrm{B,win}}(t) \equiv c'_{\mathrm{B}} \int_{\tau=t-t_{\mathrm{win}}}^{t} K_{\mathrm{B}}(t-\tau)\mathbf{g}(\tau)\mathrm{d}\tau. \tag{4}$$

Hereinafter this approach is referred to as the window method. The kernel $K_{\mathrm{B}}(t)$, however, decays very slowly for $t \to \infty$ and therefore t_{win} needs to be chosen rather large in order for $\mathbf{f}_{\mathrm{B,win}}$ to approximate $\mathbf{f}_{\mathrm{B}}$ accurately.

The Basset force can be split into two parts: the window part $\mathbf{f}_{\mathrm{B,win}}(t)$ and the remaining part (the tail part) $\mathbf{f}_{\mathrm{B,tail}}(t) \equiv \mathbf{f}_{\mathrm{B}}(t) - \mathbf{f}_{\mathrm{B,win}}(t)$. Within the framework, the window method can be considered as the approach where the Basset kernel for the tail part, K_{tail}, is set to be zero. van Hinsberg et al. (2011), on the other hand, proposed to approximate K_{tail} as

$$K_{\mathrm{tail}}(t) \approx \sum_{i=1}^{m} a_i K_i(t), \;\; K_i(t) = \sqrt{\frac{e}{t_i}} \exp\left(-\frac{t}{2t_i}\right). \tag{5}$$

Here a_i, t_i are positive constants and e is the Napier's constant. The functions $K_i(t)$ satisfy the following properties: $K_i(t_i) = K_{\mathrm{B}}(t_i)$ and $\mathrm{d}K_i(t_i)/\mathrm{d}t = \mathrm{d}K_{\mathrm{B}}(t_i)/\mathrm{d}t$. Then the tail part of the Basset history force $\mathbf{f}_{\mathrm{B,tail}}(t)$ can be expressed as:

$$\mathbf{f}_{\mathrm{B,tail}}(t) \equiv c'_{\mathrm{B}} \int_{\tau=-\infty}^{t-t_{\mathrm{win}}} K_{\mathrm{tail}}(t-\tau)\mathbf{g}(\tau)\mathrm{d}\tau \approx \sum_{i=1}^{m} a_i c'_{\mathrm{B}} \int_{\tau=-\infty}^{t-t_{\mathrm{win}}} K_i(t-\tau)\mathbf{g}(\tau)\mathrm{d}\tau = \sum_{i=1}^{m} a_i \mathbf{f}_i(t). \tag{6}$$

Table 2. List of the test cases examined in section 2.2 and the resultant absolute errors on u_p and f_B evaluated at $t \in [998\pi,\ 1000\pi]$.

Run	γ	t_w/π	$\Delta t/\pi$	f_B	error(u_p)	error(f_B)
A-1-1	3	1	1/200	eq.(6) to $f_\mathrm{B,tail}$	3.57e−3	4.26e−3
-2	3	1	1/200	$f_\mathrm{B,tail} = 0$	2.01e−2	2.84e−2
-3	3	1	1/200	$f_\mathrm{B} = 0$	1.27e−1	1.80e−1
-2-1	10	1	1/200	eq.(6) to $f_\mathrm{B,tail}$	3.10e−3	3.71e−3
-2	10	1	1/200	$f_\mathrm{B,tail} = 0$	2.65e−2	3.75e−2
-3	10	1	1/200	$f_\mathrm{B} = 0$	1.36e−1	1.92e−1
-3-1	100	1	1/200	eq.(6) to $f_\mathrm{B,tail}$	1.42e−3	1.74e−3
-2	100	1	1/200	$f_\mathrm{B,tail} = 0$	1.66e−2	2.34e−2
-3	100	1	1/200	$f_\mathrm{B} = 0$	6.41e−2	9.07e−2
-4-1	1000	1	1/200	eq.(6) to $f_\mathrm{B,tail}$	5.04e−4	6.29e−4
-2	1000	1	1/200	$f_\mathrm{B,tail} = 0$	6.55e−3	9.21e−3
-3	1000	1	1/200	$f_\mathrm{B} = 0$	2.26e−2	3.20e−2
B-1-1	3	1	1/25	eq.(6) to $f_\mathrm{B,tail}$	2.79e−2	2.76e−2
-2	3	1	1/25	$f_\mathrm{B,tail} = 0$	3.67e−2	4.30e−2
-2-1	3	1	1/100	eq.(6) to $f_\mathrm{B,tail}$	6.60e−3	7.77e−3
-2	3	1	1/100	$f_\mathrm{B,tail} = 0$	2.12e−2	2.99e−2
-3	3	1	1/200	See runs A-1.		
-4-1	3	1	1/400	eq.(6) to $f_\mathrm{B,tail}$	2.31e−3	2.62e−3
-2	3	1	1/400	$f_\mathrm{B,tail} = 0$	1.97e−2	2.79e−2
C-1-1	3	1/2	1/200	eq.(6) to $f_\mathrm{B,tail}$	3.62e−3	4.34e−3
-2	3	1/2	1/200	$f_\mathrm{B,tail} = 0$	2.93e−2	4.09e−2
-2	3	1	1/200	See runs A-1.		
-3-1	3	4	1/200	eq.(6) to $f_\mathrm{B,tail}$	3.63e−3	4.32e−3
-2	3	4	1/200	$f_\mathrm{B,tail} = 0$	1.28e−2	1.78e−2
-4-1	3	10	1/200	eq.(6) to $f_\mathrm{B,tail}$	3.57e−3	4.28e−3
-2	3	10	1/200	$f_\mathrm{B,tail} = 0$	8.50e−3	1.16e−2
-5-1	3	40	1/200	eq.(6) to $f_\mathrm{B,tail}$	5.78e−3	6.32e−3
-2	3	40	1/200	$f_\mathrm{B,tail} = 0$	5.15e−3	6.83e−3

Now $\mathbf{f}_i$ is split into two parts: $\mathbf{f}_{i-\mathrm{di}}$ that includes contributions from $\tau \in [t - t_\mathrm{win} - \Delta t, t - t_\mathrm{win}]$ (i.e., only one time step) and is directly integrated, and the remaining part $\mathbf{f}_{i-\mathrm{re}}$. The latter can be easily calculated using the value of $\mathbf{f}_i$ at the previous time step:

$$\begin{aligned}\mathbf{f}_{i-\mathrm{re}}(t) &\equiv c'_\mathrm{B} \int_{\tau=-\infty}^{t-t_\mathrm{win}-\Delta t} \sqrt{\frac{e}{t_i}} \exp\left(-\frac{t-\tau}{2t_i}\right)\mathbf{g}(\tau)\mathrm{d}\tau \\ &= \exp\left(-\frac{\Delta t}{2t_i}\right) c'_\mathrm{B} \int_{\tau=-\infty}^{(t-\Delta t)-t_\mathrm{win}} \sqrt{\frac{e}{t_i}} \exp\left(-\frac{(t-\Delta t)-\tau}{2t_i}\right)\mathbf{g}(\tau)\mathrm{d}\tau = \exp\left(-\frac{\Delta t}{2t_i}\right)\mathbf{f}_i(t-\Delta t). \quad (7)\end{aligned}$$

By utilizing the recursive formulation of eq. (7), contributions from the interval $[-\infty, t - t_\mathrm{win} - \Delta t]$ to the Basset history force $\mathbf{f}_\mathrm{B}$ can be included with no explicit integration over the interval.

Look at van Hinsberg et al. (2011) for details of numerical integration of $\mathbf{f}_{\mathrm{B,win}}$ and $\mathbf{f}_{i-\mathrm{di}}$. Coefficients a_i and $\tilde{t}_i$ ($\equiv t_i/t_\mathrm{win}$) are presented for $m = 10$ in the paper, and those values were employed in the present study.

2.2 Validation of the method

Here accuracy and efficiency of the method proposed by van Hinsberg et al. (2011) has been critically examined. An ordinary differential equation of the form

$$\frac{du_\mathrm{p}}{dt} = a\frac{du_\mathrm{f}}{dt} + b(u_\mathrm{f} - u_\mathrm{p}) + \frac{c}{\sqrt{\pi}} \int_{\tau=-\infty}^{t} \frac{1}{\sqrt{t-\tau}} \left\{ \frac{du_\mathrm{f}(\tau)}{d\tau} - \frac{du_\mathrm{p}(\tau)}{d\tau} \right\} \mathrm{d}\tau \quad (8)$$

has, under the condition of $u_\mathrm{f}(t) = \sin t$, the theoretical solution (Sugiyama et al., 2004)

$$u_\mathrm{p}(t) = v_\mathrm{c} \cos t + v_\mathrm{s} \sin t, \quad (9)$$

and the Basset force (the third term on the RHS of eq. (8)) can be expressed as

$$\frac{1}{\sqrt{\pi}} \int_{\tau=-\infty}^{t} \frac{1}{\sqrt{t-\tau}} \left\{ \frac{du_\mathrm{f}(\tau)}{d\tau} - \frac{du_\mathrm{p}(\tau)}{d\tau} \right\} \mathrm{d}\tau = \frac{1 - v_\mathrm{c} - v_\mathrm{s}}{\sqrt{2}} \cos t + \frac{1 + v_\mathrm{c} - v_\mathrm{s}}{\sqrt{2}} \sin t. \quad (10)$$

Here v_c and v_s are given by

$$v_c = \frac{1}{D}\left(ab + \frac{ac}{\sqrt{2}} - b - \frac{c}{\sqrt{2}}\right),\ v_s = \frac{1}{D}\left(a + \frac{ac}{\sqrt{2}} + b^2 + \sqrt{2}bc + c^2 + \frac{c}{\sqrt{2}}\right), \tag{11}$$

$$D = b^2 + \sqrt{2}bc + c^2 + \sqrt{2}c + 1. \tag{12}$$

Eq. (8) corresponds to eq. (2) with $g = 0$ when $a = \beta$, $b = 1/\tau_p^*$, and $c = \sqrt{3ab}$. In the following, we consider the case of $\tau_p^* = 2\pi$, i.e., the effective particle relaxation time τ_p^* is equal to the oscillation period of the fluid velocity u_f.

We have performed 26 different runs in total. Table 2 compiles the physical and numerical conditions, and the root-mean-square errors in the particle velocity u_p and the Basset history force f_B obtained from each run. Since the lower limit of the integral in eq. (8) is $-\infty$, the time integration must be carried out for a long period of time. Here it was chosen to be 1000π (i.e., 500 oscillation periods in u_f), and the errors presented in table 2 were evaluated at $t \in [998\pi,\ 1000\pi]$. The present investigation can be split into three cases: the influence of [A] the particle-to-fluid mass density ratio γ, [B] the time increment Δt, and [C] the length of time interval t_{win} for the window part of the Basset force, $\mathbf{f}_{B,win}$, were examined critically.

In runs A, the mass density ratio γ was changed between 3 and 1000, and the Basset force was (i) approximated by the method of van Hinsberg et al. (2011), (ii) approximated by the window method (i.e., $f_{B,tail} = 0$), or (iii) neglected totally. Figure 1 shows the time evolutions of the solution u_p (left panels) and each term of eq. (8) for $t \in [998\pi,\ 1000\pi]$, along with the theoretical solutions. In the left panels, u_p obtained from (i), (ii), and (iii) explained above are shown together. In the right panels, on the other hand, only the results from (i) are presented. It can be clearly seen from the right panels in figure 1 that, with decrease in the mass density ratio γ, first the Basset history force becomes no more negligible and then the pressure-gradient force gets comparable to the Stokes drag force. This behavior is in exact accordance with the argument derived from table 1. The left panels clearly reveal the importance of the Basset force to reproduce the particle behavior accurately at $\gamma \leq 100$. In the following, we fix our attention to the case of $\gamma = 3$, where all the terms in eq. (8) are non-negligible.

The influence of the time increment Δt on the prediction results was examined in runs B. Table 2 shows that, with van Hinsberg's method, the use of small Δt yields accurate evaluation of the Basset force and hence the particle velocity u_p. It, however, does not with the window method, since, with decrease in Δt, the tail part of the Basset history force $f_{B,tail}$ becomes larger than the error produced in the numerical integration of the window part $f_{B,win}$.

Finally the effect of t_{win} was investigated in runs C. While the prediction accuracy of u_p gets worse with decrease in t_{win} by means of the window method, it is quite independent of the choice of t_{win} with van Hinsberg's method. It is noteworthy that van Hinsberg's method with $t_{win} = \pi/2$ gives better prediction than the window method with $t_{win} = 40\pi$. It has been clearly demonstrated in the results obtained from runs B and C that van Hinsberg's method has a clear superiority to the traditional window method in providing an accurate prediction with much less time and memory requirements.

3. PHYSICAL AND NUMERICAL DETAILS

We numerically solved the incompressible Navier-Stokes equations in a periodic box by the Fourier spectral method and obtain homogeneous isotropic turbulence (HIT). Artificial forcing was implemented to maintain the statistical stationarity of the turbulence (Yamazaki et al., 2002). Here a HIT of the Taylor Reynolds number Re_λ of about 42 was reproduced with 48^3 Fourier modes.

We assume that particles do not disturb the fluid flow and do not interact with other particles as well (one-way coupling). We put different types of particles in the flow. Each type consists of 1.5×48^3 particles with the same physical properties. The particle Stokes number based on the Kolmogorov time scale $S_\eta \equiv \tau_p^*/\tau_\eta$ is unity, and the gravity effect is neglected in the present study. The mass density ratio γ was changed systematically from 0 up to 10000, which covers a wide range of conditions from the ultimately light particle to a very heavy particle. The particles in a type were initially seeded at random locations through the computational domain, and the initial distribution was applied to other types as well. The initial particle velocity was set to be the local fluid velocity.

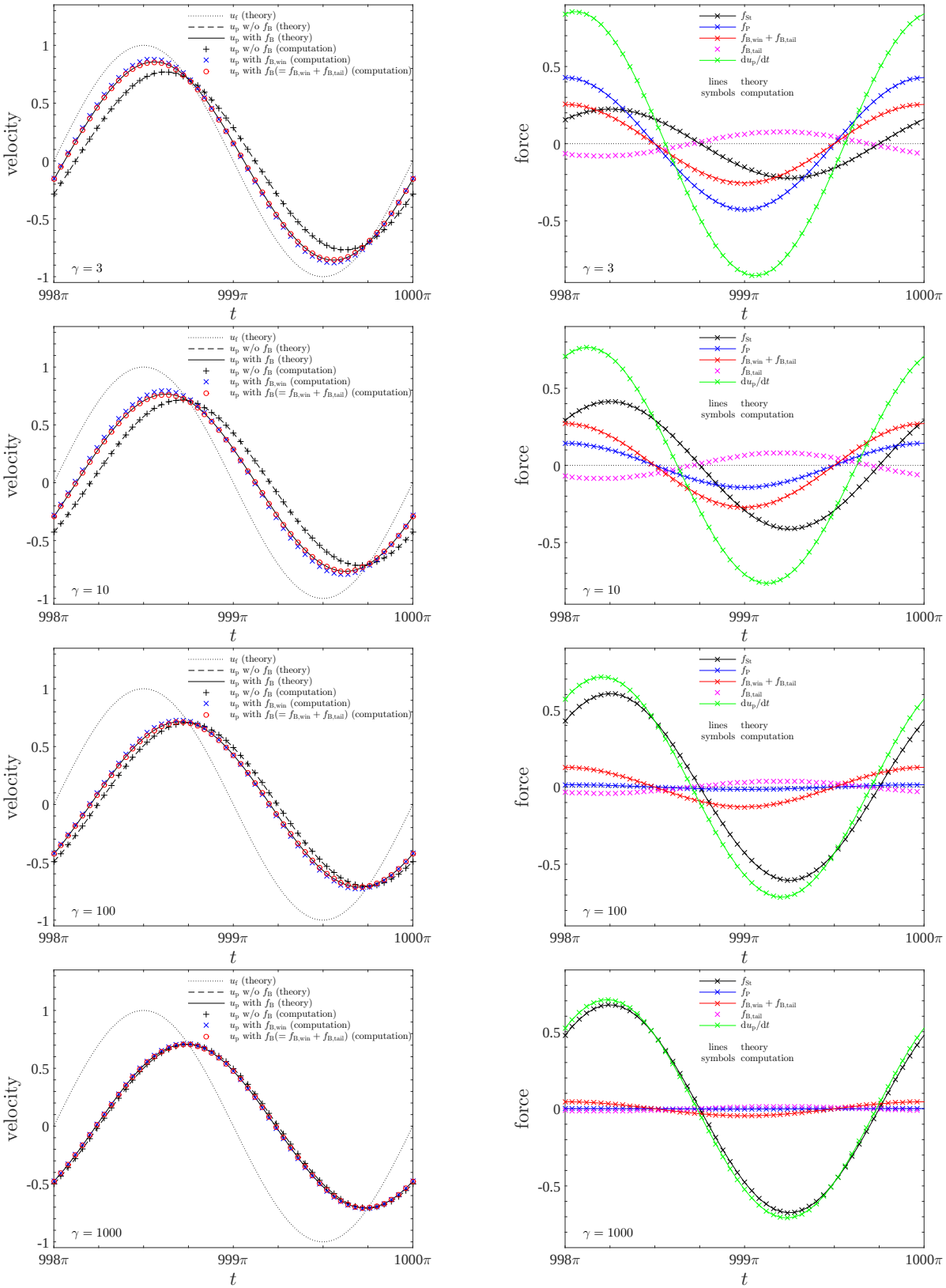

Figure 1. Time evolutions of the solution u_p (left) and of each of the terms (right) of eq. (8), over $t \in [998\pi,\ 1000\pi]$.

4. RESULTS AND DISCUSSION

4.1 Incluence of numerical approximation to Basset history force

Here we show the importance of accurately calculating the Basset history force for clarification of the physics of preferential concentration phenomena. We compared the computational results by means of van Hinsberg's method and the window method to approximate the Basset history force. Note that the window part of the Basset history force $\mathbf{f}_{B,win}$ was evaluated by the same method proposed in van Hinsberg et al. (2011) in both approaches. We focus on the case of $\gamma = 3$, where all the terms in the

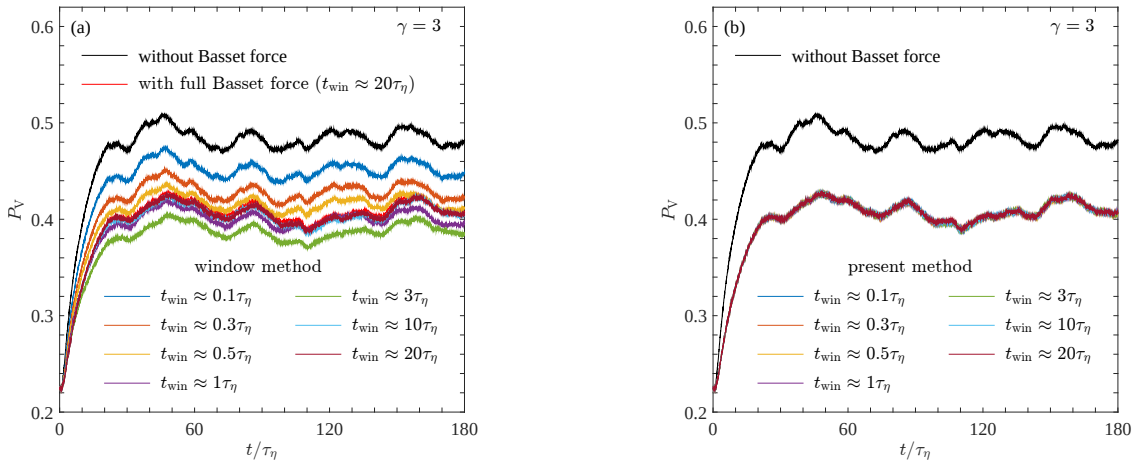

Figure 2. Influence of parameter $t_{\rm win}$ that defines the extent of contribution from $\mathbf{f}_{\rm B,win}$, on the particle void fraction $P_{\rm v}$. (a): window method; (b): method by van Hinsberg et al. (2011).

MR equation are non-neglibigle. The parameter $t_{\rm win}$ that defines the extent of contribution from the window part was changed as $t_{\rm win}/\tau_\eta \approx 0.1, 0.3, 0.5, 1, 3, 10$ and 20. These values of $t_{\rm win}$ correspond to $3, 10, 17, 33, 100, 333$ and 667 time steps, respectively.

To describe quantitatively the extent of nonuniformity in particle distribution, here we introduced the particle void fraction $P_{\rm v}$ (Yoshimoto and Goto, 2007). $P_{\rm v}$ represents the ratio of the computational cells containing no particles. Figure 2 shows the time evolutions of $P_{\rm v}$. When van Hinsberg's method was used to calculate the Basset force, the $P_{\rm v}$ profile was found to be totally independent of the choice of $t_{\rm win}$ (figure 2(b)). With the traditional window method, on the other hand, the results show strong dependence on $t_{\rm win}$ (figure 2(a)). The computational result using van Hinsberg's method with $t_{\rm win} \approx 20\tau_\eta$, i.e., a fully converged solution, was included in figure 2(a) for comparison. It can be seen that the window method showed a non-monotonic convergence behavior with increase in $t_{\rm win}$ and did not reach the well-converged solution even with $t_{\rm win} \approx 20\tau_\eta$. It means that a caution is needed in reliability of the results based on the window method. van Aartrijk and Clercx (2010) pointed out that $t_{\rm win} \approx 2\tau_\eta$ was enough to obtain a well-converged solution by the window method in stably stratified turbulence. The present study showed stronger dependence on $t_{\rm win}$ than the previous study.

Hereinafter the computational results by van Hinsberg's method with $t_{\rm win} \approx 1\tau_\eta$ will be treated as "with Basset history force".

4.2 Influence of Basset history force on preferential concentration of small particles and bubbles

Figure 3 shows the time evolutions of $P_{\rm V}$ at various mass density ratio γ, from 0 up to 10000. Figure 4 presents instantaneous snapshots of spatial distribution of each type of particles. It is clearly shown from both $P_{\rm V}$ profiles and the spatial distributions of particles that, when the particle is very heavy (i.e., $\gamma \geq 1000$) or is almost neutrally buoyant ($\gamma \approx 1$), the extent of preferential concentration of particles is not affected by the Basset history force. Otherwise, the presence of the Basset history force weakens the level of preferential concentration, especially under the conditions of $\gamma \sim 1.5-10$ for heavy particles and $\gamma \leq 0.7$ for light particles.

Finally, the relation between the particle distribution and the coherent vortical structures was investigated. Figure 5 presents the spatial distribution of particles together with the profile of the second invariant of the velocity-gradient tensor Q, for $\gamma = 0$ (ultimately light particle) and $\gamma = 10000$ (very heavy particle). As has been explained in previous studies (e.g., Yoshimoto and Goto, 2007), heavy particles tend to be swept out of intense eddies (where $Q > 0$, rotation-dominated regions) due to centrifugal effects and accumulate along the outer peripheries of eddies. Light particles, on the other hand, tend to accumulate inside eddies. This trend of spatial distribution of light particles was considerably relaxed by the presence of the Basset history force.

REFERENCES

van Aartrijk, M. and Clercx, H. J. H. (2010). Vertical dispersion of light inertial particles in stably stratified turbulence: The influence of the Basset force. *Phys. Fluids*, 22: 013301.

Bombardelli, F. A., González, A. E. and Niño, Y. I. (2008). Computation of the particle Basset force with a

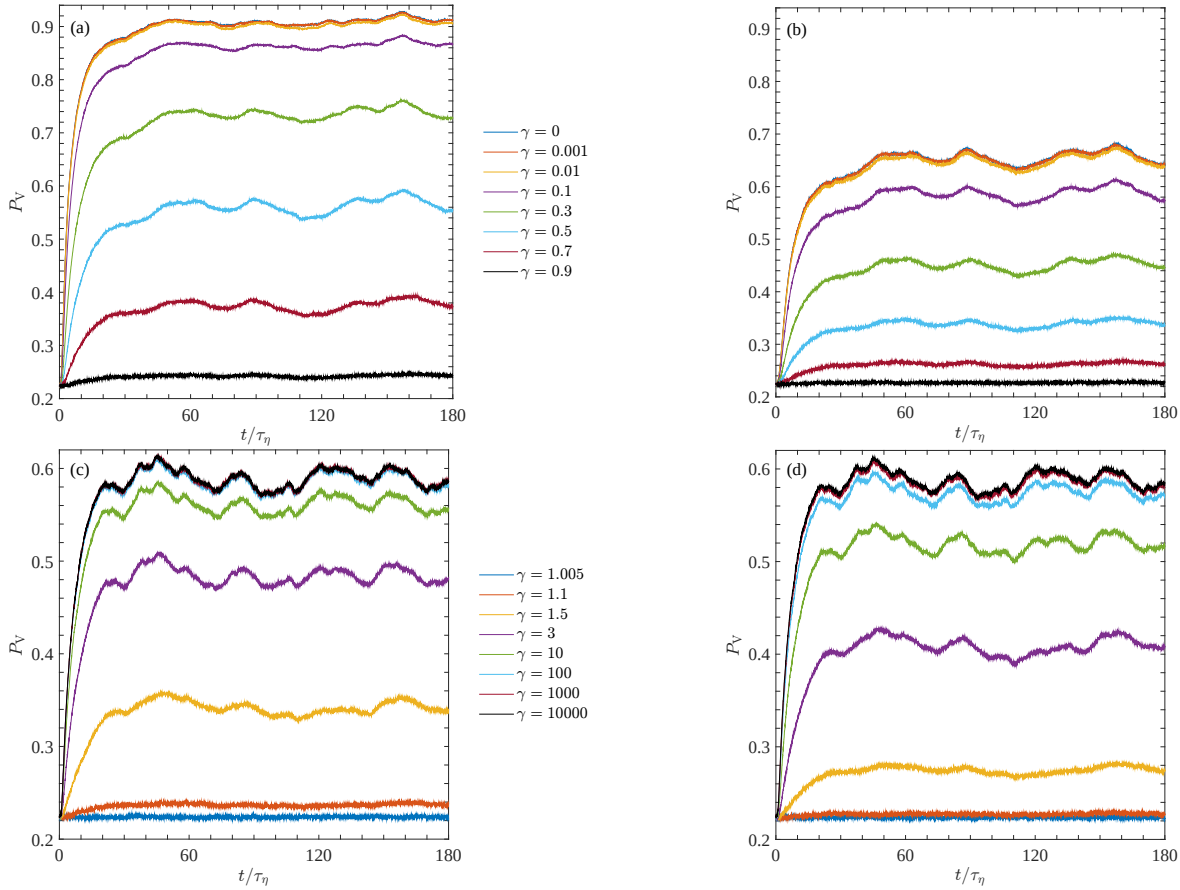

Figure 3. Influence of mass density ratio γ on the particle void fraction P_v. (a),(b): light particles ($\gamma < 1.0$); (c),(d): heavy particles ($\gamma > 1.0$). (a),(c): without Basset force; (b),(d): with Basset force.

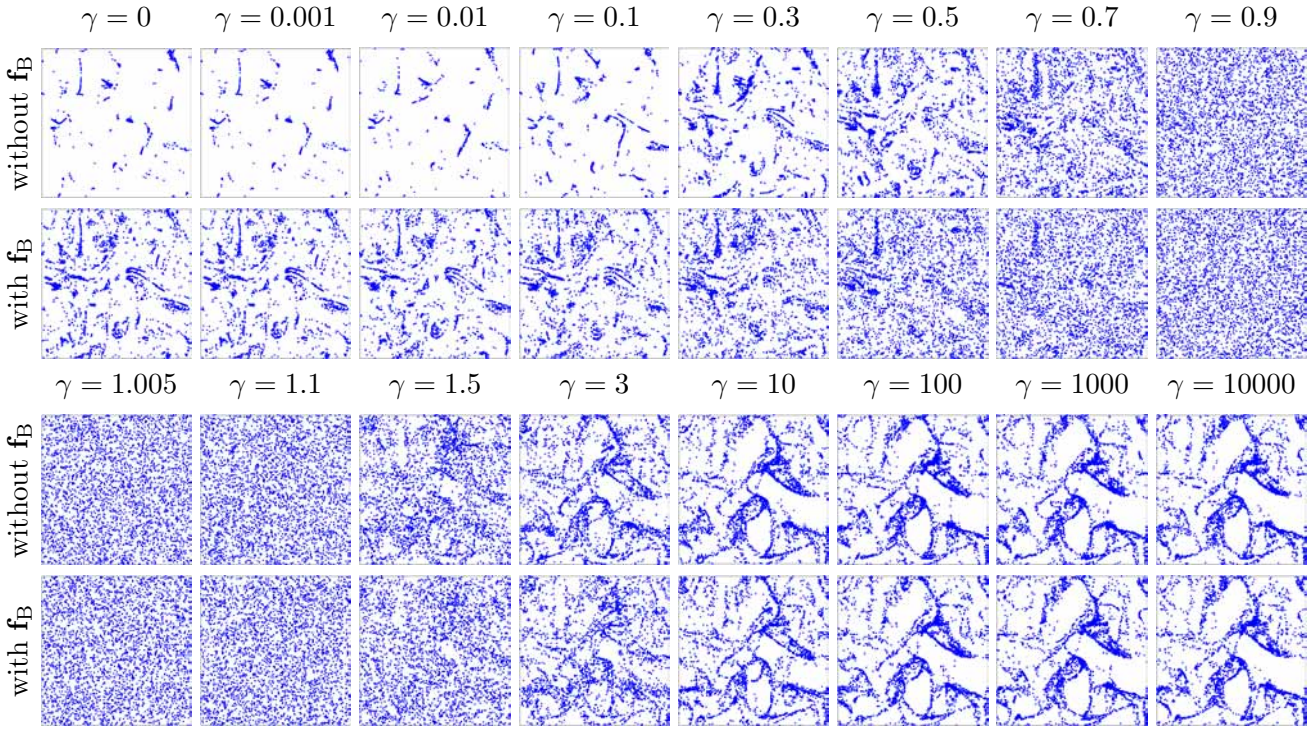

Figure 4. Influence of mass density ratio γ on instantaneous spatial distribution of particles inside a thin layer (side length 108.8η and depth 2.3η, where η denotes the Kolmogorov length).

fractional-derivative approach. *J. Hydraul. Eng. ASCE*, 134: 1513–1520.

Maxey, M. R. and Riley, J. J. (1983). Equation of motion for a small rigid sphere in a nonuniform flow. *Phys. Fluids*, 26: 883–889.

Sugiyama, K., Takagi, S. and Matsumoto, Y. (2004). Effect of the history force on the translational motion of bubbles and particles in cellular flow. *Trans. JSME*, 70-699B: 2738–2747. [In Japanese]

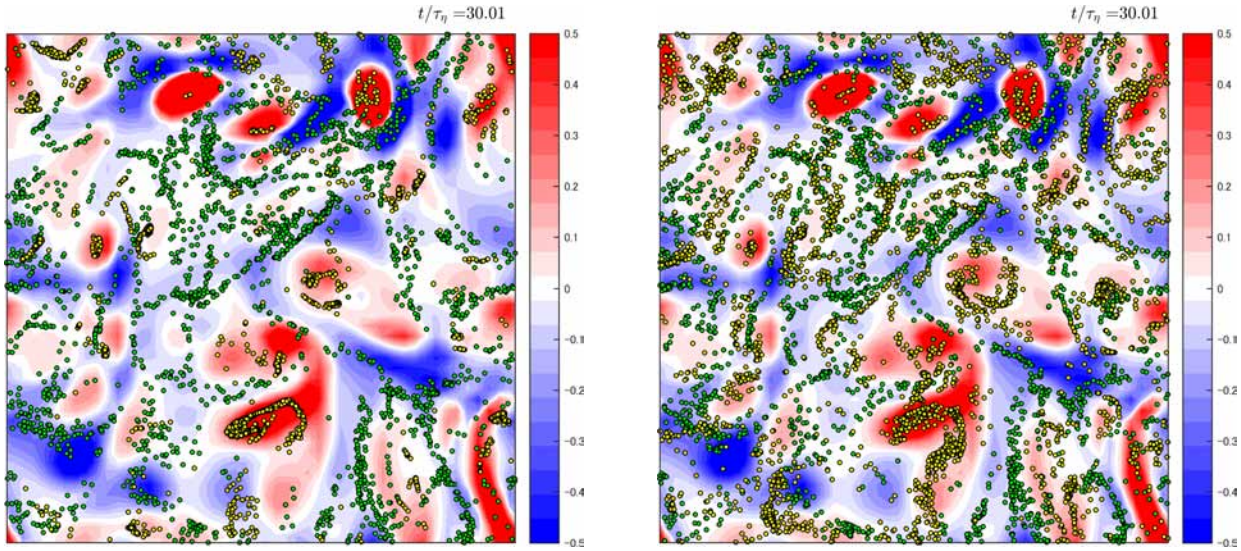

Figure 5. Relation between spatial distribution of particles (green: very heavy particle $\gamma = 10000$; yellow: ultimately light particle $\gamma = 0$) and coherent vortical structures in homogeneous turbulence visualized by color contours of the second invariant of the velocity-gradient tensor normalized by the Kolmogorov scale. Left: without Basset force; right: with Basset force.

van Hinsberg, M. A. T., Clercx, H. J. H. and Toschi, F. (2017). Enhanced settling of nonheavy inertial particles in homogeneous isotropic turbulence: The role of the pressure gradient and the Basset history force. *Phys. Rev. E* 95: 023106.

van Hinsberg, M. A. T., ten Thije Boonkkamp, J. H. M. and Clercx, H. J. H. (2011). An efficient, second order method for the approximation of the Basset history force. *J. Comput. Phys.* 230: 1465–1478.

Yamazaki, Y., Ishihara, T. and Kaneda, Y. (2002). Effects of wavenumber truncation on high-resolution direct numerical simulation of turbulence. *J. Phys. Soc. Jpn.*, 71: 777–781.

Yoshimoto, H. and Goto, S. (2007). Self-similar clustering of inertial particles in homogeneous turbulence. *J. Fluid Mech.*, 577: 275–286.